

ρ^0 Photoproduction in Ultra Peripheral Relativistic Heavy Ion Collisions with STAR

XX YY*

(Dated: June 8, 2007)

Photoproduction reactions can occur when the electromagnetic field of a relativistic heavy-ion interacts with another heavy ion. The STAR collaboration presents a measurement of ρ^0 and direct $\pi^+\pi^-$ photo-production in ultra peripheral relativistic heavy ion collisions at $\sqrt{s_{NN}}=200$ GeV. We observe both exclusive photoproduction and photoproduction accompanied by mutual Coulomb excitation; we find a coherent cross-section of $\sigma(AuAu \rightarrow AuAu\rho) = 509 \pm 34 \pm 107$ mb, in accord with theoretical calculations based on the Glauber model, but considerably below the predictions of a parton saturation model. The ρ transverse momentum spectrum is fit by a model including both coherent and incoherent coupling to the target nucleus; we find $\sigma_{inc}/\sigma_{coh} = 0.29 \pm 0.03 \pm 0.03$. The ratio of ρ to direct $\pi\pi$ production is comparable to that observed in γp collisions at HERA, and appears to be independent of photon energy. The ρ^0 spin helicity matrix elements have been measured. Helicity is conserved within errors as expected based on s-channel helicity conservation.

PACS numbers: Valid PACS appear here

I. INTRODUCTION

Photoproduction occurs in heavy-ion collisions when the electromagnetic field of one nucleus interacts with the other [1]. The electromagnetic field may be represented as a flux of almost-real virtual photons, following the Weizsäcker-Williams method [2]. The photon flux scales as the nuclear charge, Z , squared, so the cross-sections can be large. This photoproduction is visible in ultra-peripheral collisions (UPCs), which occur when the impact parameter b is more than twice the nuclear radius R_A , so no hadronic interactions occur.

ρ^0 photoproduction occurs when the photon fluctuates to a quark-antiquark pair, which then scatters elastically from the target nucleus, emerging as a ρ . The elastic scattering can be treated as being due to Pomeron exchange. ρ photoproduction on nuclear targets has been studied at fixed target accelerators [3] and by the STAR collaboration [4]; J/ψ photoproduction has been studied by the PHENIX collaboration [5].

The ρ production cross-section depends on the $q\bar{q}$ coupling to the nuclear target. For ρ production at large transverse momentum, p_T , the $q\bar{q}$ pair couples to an individual nucleon; this is known as incoherent photoproduction. The incoherent cross-section scales roughly as the atomic number A , minus a correction due to nuclear absorption of the ρ .

At smaller p_T , roughly $p_T < \hbar/R_A$, the $q\bar{q}$ pair couples coherently to the entire nucleus; naively, this leads to a cross-section that scales as A^2 . However, absorption corrections reduce this to a roughly $A^{5/3}$ dependence for the ρ^0 . The coherent production is regulated by the nuclear form factor $F(t)$.

ρ photoproduction is sensitive to the ρ -nucleon interaction cross-section and the nuclear structure functions. There are three published calculations of the coherent ρ^0

photoproduction cross-section in heavy-ion collisions.

The first model (Klein-Nystrand, KN), uses vector meson dominance (VMD) plus a classical mechanical approach for nuclear scattering and uses information from the $\gamma P \rightarrow Vp$ experiments for extrapolation [6]; in 200 GeV per nucleon gold-gold collisions, it predicts a total coherent ρ photoproduction cross section $\sigma_{\rho^0}=590$ mb. The second model (Frankfurt-Strikman-Zhalov, FSZ) treats the ρ production using the generalized quantum VMD and the Gribov-Glauber approach [7]; it predicts $\sigma_{\rho^0}=934$ mb [8], about 50 % higher than the first model, but with a similar rapidity distribution. The third model (Goncalves-Machado - GM) describes the photoproduction of the vector mesons in UPC events using the QCD color dipole approach [9]. This model includes nuclear effects and parton saturation phenomena. It finds $\sigma_{\rho^0}=876$ mb , but with a very different rapidity distribution from the other models.

The second and third theoretical models provide predictions for the momentum transfer dependence of both coherent and incoherent ρ -meson production.

Previous fixed-target photoproduction experiments with nuclear targets were at much lower γN collision energies [3]. The STAR collaboration has published measurements of the ρ^0 production cross section at a center of mass energy $\sqrt{s_{NN}} = 130$ GeV per nucleon [4]. This work is at a higher center of mass energy, 200 GeV per nucleon. At mid-rapidity, this corresponds to a photon energy of about 70 GeV in the target frame, and a γ -nucleon center of mass energy, $W_{\gamma N}$, of about 12 GeV. In the laboratory frame, the photon energy required to produce a vector meson with mass m_V at rapidity y_ρ is

$$k = \frac{m_V}{2} \exp(\pm y_\rho). \quad (1)$$

The two signs are due to the two-fold ambiguity over which nucleus emitted the photon. Away from mid-rapidity, most of the ρ^0 production comes from the solution with the lowest photon energy.

The target-frame kinematics depend on the beam Lorentz boost, γ ; $\gamma = 108$ at RHIC. In the target frame,

*Also at Physics Department, XYZ University.

the photon energy is 2γ times higher, and $W_{\gamma N}$ is about $12 \exp(\pm y)$ GeV. The energy range corresponding to $|y_{\rho^0}| < 1$ is $4 < W_{\gamma N} < 33$ GeV, somewhat above the reach of γA fixed target experiments.

This study has about 10 times the statistics as the previous STAR study, allowing more precise measurements of the cross-sections. We measure both coherent and incoherent photoproduction, and also the spin-matrix elements of the ρ production.

In addition to exclusive ρ photoproduction, we have studied ρ photoproduction accompanied by mutual Coulomb excitation, as is shown in Fig. 1. This process primarily occurs via 3-photon exchange, with one photon producing the ρ , and one exciting each nucleus [10, 11]. Each single-photon reaction is independent, and the cross-sections may be written as an integral over the impact parameter

$$\begin{aligned} \sigma(AuAu \rightarrow Au^*Au^*\rho) = \\ = \int d^2b [1 - P_{Had}(b)] P_\rho(b) P_{Xn1}(b) P_{Xn2}(b) \end{aligned} \quad (2)$$

where $P_{Had}(b)$ is the probability of a hadronic interaction, $P_\rho(b)$ is the probability to produce a ρ , and $P_{Xn1}(b)$ and $P_{Xn2}(b)$ are the probabilities to excite nucleus 1 and 2 respectively. In mutual Coulomb excitation, the nuclei decay primarily by channels involving neutron emission. This is attractive experimentally, since the neutrons provide simple trigger signals. The three-photon exchange reactions are biased toward smaller impact parameters than single-photon reactions, leading to a harder photon spectrum and an altered rapidity distribution.

One particular nuclear excitation merits special interest: excitation to a Giant Dipole Resonance (GDR), which involves particularly low-energy photons. Single GDR is the main contribution in the total fragmentation cross section induced by Coulomb excitation in UPC. GDRs usually decay by single neutron emission, which is considered to be a major source of the beam losses in the heavy ion colliders [12].

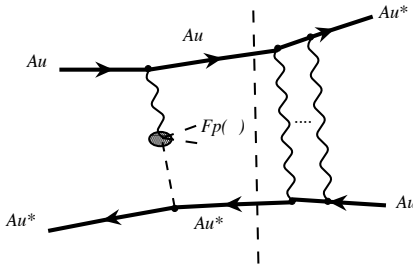


FIG. 1: The diagrams for ρ photoproduction accompanied by mutual Coulomb excitation. The latter process primarily via 3-photon exchange; the dashed line shows how the photoproduction factorizes from the mutual Coulomb excitation.

The differential production cross section of the vector mesons and the vector-meson decay angular distribution

can be expressed as functions of the vector-meson density matrix, which is represented by the sum of the helicity states [13]. Three ρ^0 spin density matrix elements were measured for $p_T < 150$ MeV and photon-nucleon center-of-mass system $W_{\gamma N} \approx 10$ GeV, not covered by the previous fixed target experiments [14].

II. EXPERIMENTAL SETUP AND TRIGGERING

This data was taken with the Solenoidal Tracker at RHIC (Relativistic Heavy Ion Collider)[STAR] at Brookhaven National Laboratory during the 2001 run. Gold nuclei collided at $\sqrt{S_{NN}}=200$ GeV. Charged particle tracks were reconstructed in a cylindrical Time Projection Chamber (TPC). The TPC is a 4.2 m long barrel with a 2 m radius operated in a solenoidal magnetic field of 0.5 T [15]. The TPC detected charged tracks with pseudorapidity $|\eta| < 1.2$ and $p_T > 100$ MeV with good efficiency. The TPC is surrounded by 240 CTB (Central Trigger Barrel) slats. Two ZDC (Zero Degree Calorimeters) are situated along the beam pipe at ± 18 m from the interaction point. They have an acceptance close to unity for the neutrons originating from nuclear break-up.

This analysis used data from two triggers: a topology trigger and a minimum bias trigger. The topology trigger uses the CTB detector. The CTB was divided into four azimuthal quadrants. A coincidence between the side quadrants was required, and the top and bottom quadrants were required to be empty. The veto was used to reduce the trigger rate due to cosmic ray muons.

The minimum bias trigger required a coincidence in the ZDCs; it was sensitive to photoproduction accompanied by mutual Coulomb excitation. By eliminating cosmic-rays and other extraneous interactions, this trigger had considerably better selectivity than the topology trigger. The ZDCs have sufficient energy resolution to count the number of neutrons present. We distinguish between several different excitation modes: XnXn - at least one neutron in each of the ZDC detectors, 1n1n - exactly one neutron in each of the ZDC detectors, 0nXn - at least one neutron in one of the ZDC detectors and none in the other and 0n0n - no neutrons in either ZDC. The last two modes are only accessible in the topology trigger. A typical ZDC spectrum is shown in the Fig. 2. This spectrum allows us to measure the cross section for different excitation states.

III. ρ^0 PHOTOPRODUCTION

A. Event Selection

This analysis selected events with two oppositely charged tracks forming a primary vertex and less than 5 reconstructed charged tracks per event. A ρ photoproduction event should have exactly two tracks in the TPC,

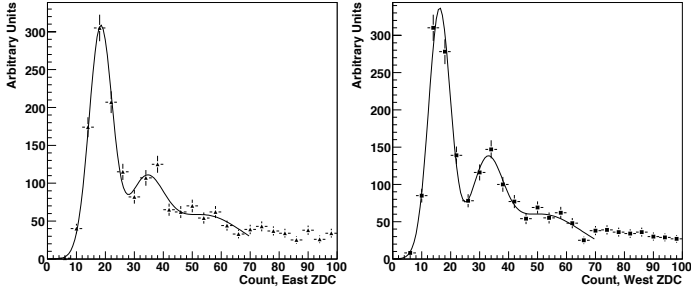


FIG. 2: ZDC spectra obtained with the minimum bias sample after the ρ^0 selection cuts are applied, fitted with three Gaussians: east ZDC - left, west ZDC - right. The ratio of number of candidates in the 1n:2n:3n peaks is 2.4:1.1:1.0.

but additional tracks may come from overlapping interactions, including beam-gas events. The STAR TPC has a $36\mu\text{s}$ drift time, so any charged particles traversing the TPC within $\pm 36\mu\text{s}$ may deposit energy which overlaps with the tracks of interest. We accounted for the effect of these tracks in our analysis by allowing for varying numbers of total tracks in the event, which encompass both primary and secondary tracks. The selected events may contain up to 3 secondary tracks along with 2 primary tracks. When the cut on the total number of tracks was relaxed from 2 to 5, the number of included events increased by 27 %; our results are corrected by this factor.

The reconstruction software formed a vertex from charged particle multiplets arising near the origin, using a low multiplicity vertexing. The single track reconstruction efficiency for $|y| < 1$ is about 85 %, and the vertex finding efficiency for a two-track vertex is 80 ± 8 %.

There are several types of backgrounds: peripheral hadronic interactions, other photonuclear interactions, e^+e^- pairs from two-photon interactions, and unrelated processes such as beam gas interactions, cosmic-ray muons or pile-up events. These backgrounds can be reduced by cuts on the total multiplicity, vertex position, and other event characteristics.

The multiplicity cut suppresses the contribution from hadronic and pile-up events. In order to reduce the backgrounds originated from processes like beam gas, upstream interactions, cosmic-rays and pile-up events. We selected events with vertices within 15 cm radially and 100 cm longitudinally (along the beam direction) of the center of the interaction region. Those two cuts reject approximately 25 % of the events. We also required that tracks be formed from at least 14 hits in the TPC (out of 45 layers in the TPC). This cut has a similar rejection factor of 1.3. In order to retain as much as possible of the incoherently produced ρ^0 mesons while removing combinatorial background, a relatively soft cut on the transverse momentum ($p_T \leq 550$ MeV) is applied.

This analysis uses events with a $\pi\pi$ invariant mass, $M_{\pi\pi}$, between 500 and 1100 MeV. The lower cutoff eliminates the e^+e^- pairs from two-photon interactions [16] that were a small background in the 130 GeV analysis.

Even with the trigger veto, some cosmic-ray muons remain in the topology sample. Muons that pass near the interaction region may be reconstructed as a pair of tracks with net charge 0, net $p_T \approx 0$ and $y_{\rho^0} \approx 0$. These muons are removed by applying a cut on the rapidity, $|y_{\rho^0}| > 0.01$. The ZDC energy deposition requirements largely eliminate cosmic-ray contamination in the minimum bias sample.

We use several approaches to estimate the remaining backgrounds. As with the 130 GeV analysis, like-sign pairs ($\pi^+\pi^+$ and $\pi^-\pi^-$) provide a good background model. That analysis only considered coherent ρ^0 production; the like-sign background was scaled up by a factor of 2.1-2.3 to match the data at high p_T . By definition, this treats incoherent ρ production as a background. We use this approach for the $|B/A|$ ratio of ρ^0 to direct $\pi^+\pi^-$ production measurement for the coherently produced ρ^0 mesons in this analysis, since it correctly estimates the combinatorial background. For the rest of the measurements, we use the unscaled background in order to retain the incoherent ρ^0 signal. A background model comes by including a polynomial background in our fits to the $M_{\pi\pi}$ spectrum. The polynomial function is initialized with parameters obtained from the fit of the polynomial function to the non scaled like-sign distribution. These different approaches for the background description causes a 3 % systematic error.

B. Efficiency and Acceptance Determination

The acceptance of the detector was studied using Monte Carlo [6, 10] generated events which reproduce the kinematical and geometrical properties of the ρ^0 mesons produced via coherent photoproduction. These events were passed through a realistic detector simulation which reproduces detector resolution and efficiency. The efficiency calculation includes the detector acceptance, track and vertex reconstruction efficiency and selection cuts.

The efficiency was studied as a function of p_T , p_T^2 , Φ , Θ , y_ρ^0 and $M_{\pi^+\pi^-}$. The efficiency for minimum bias Monte Carlo ρ^0 with $|y_\rho^0| < 1$ is 44 ± 5 %. This efficiency is relatively constant with respect to p_T and azimuthal angle, but drops as $|y_\rho^0|$ increases, due to the TPC acceptance. The Monte Carlo efficiency for topology-triggered ρ^0 with $|y_\rho^0| < 1$ is 11 ± 1 %. For these events, the efficiency drops slowly as p_T or $|y_\rho|$ rises; there is also a large azimuthal asymmetry due to the topology trigger veto regions.

The estimated resolution for p_T , y_ρ and $M_{\pi^+\pi^-}$ are approximately 6 MeV, 0.01 and 6 MeV respectively for track pairs which passed through the ρ^0 selection cuts.

C. Luminosity

The luminosity for the minimum bias data sample is calculated by assuming that the main contribution arises

from hadronic production, with a known cross section. The luminosity was measured by counting events with at least 14 tracks with $p_T \leq 0.1$ GeV and $|y_\rho| \leq 0.5$. These events correspond to 80 % of the total hadronic production cross section of 7.2 b [17]. An extra correction is required to remove the effects of an unstable dead time caused by the SVT (Silicon Vertex Detector). The integrated luminosity of the minimum bias sample is measured to be $L = 461.3 \text{ mb}^{-1}$ with a systematic uncertainty of 10 %. The systematic is due largely to uncertainty of the gold-gold hadronic cross section.

D. Invariat Mass Fit Function

The invariant mass distribution of track pairs was found by assuming that all reconstructed particles were pions - no particle identification was applied. The invariant mass distributions for the minimum bias and topology samples are shown in Fig. 3. After cuts, the minimum bias sample contains 5,011 selected events, while the topology sample contains 14,693 selected candidates.

$\pi^+\pi^-$ pairs may be photoproduced via the ρ^0 , or the photon may fluctuate directly to $\pi^+\pi^-$. The latter produces a flat $M_{\pi^+\pi^-}$ mass distribution. The two experimentally indistinguishable processes interfere; the interference is constructive for $M_{\pi\pi} < M_\rho$ and destructive for $M_{\pi\pi} > M_\rho$ [18].

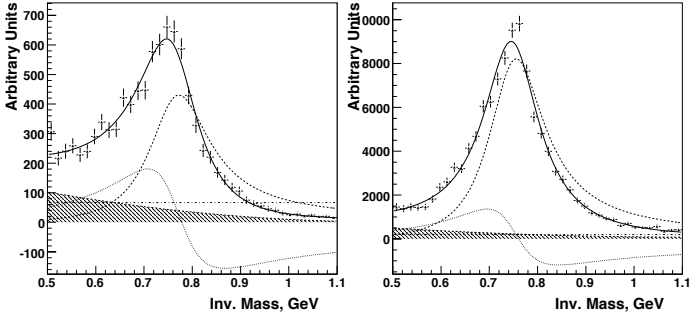


FIG. 3: Left: Invariant mass distribution for the coherently produced ρ^0 candidates from the minimum bias sample with $p_T < 150$ MeV. Right: Invariant mass distribution for the coherent produced ρ^0 candidates obtained from the topology sample with $p_T < 150$ MeV. The hatched histogram is the contribution from the combinatorial background. The solid line corresponds to the Eq. 3 which encompass Breit-Wigner (dashed), the mass independent contribution from the direct $\pi^+\pi^-$ production (dash-dotted) and their interference (dotted).

The invariant mass distribution of the ρ candidates has been fitted with a relativistic Breit-Wigner [19] function plus a contribution for the direct $\pi^+\pi^-$ production and an interference (Söding) term [20, 21]. The background is described by a 2nd order polynomial. The estimation of the background from the like sign pairs has been used to obtain the initial parameters of the polynomial function.

The fit function is:

$$\frac{dN}{dM_{\pi\pi}} = \left| A \frac{\sqrt{M_{\pi\pi} M_\rho \Gamma_\rho}}{M_{\pi\pi}^2 - M_\rho^2 + i M_\rho \Gamma_\rho} + B \right|^2 + f_p, \quad (3)$$

where

$\Gamma_\rho = \Gamma_0 \cdot (M_\rho/M_{\pi\pi}) \cdot [(M_{\pi\pi}^2 - 4m_\pi^2)/(M_\rho^2 - 4m_\pi^2)]^{3/2}$ is the momentum-dependent width and M_ρ is the mass of the ρ^0 , A is the amplitude for the Breit-Wigner function, B is the amplitude for the direct $\pi^+\pi^-$ production and f_p is the fixed second order polynomial which used to describe background. For the minimum bias data set the width and mass position for the ρ^0 agree with PDG [22] values. The difference between the yield obtained with fixed ρ^0 width and mass position from those obtained without fixing the width and position is about 2 %. In addition, fixing the width leads to an increase in the χ^2/NDF to up to 5 %. Using the above mentioned fit procedure, the minimum bias sample contains $3,075 \pm 128 \rho^0$ candidates, while the topology sample contains $13,054 \pm 124 \rho^0$ candidates.

For the minimum bias data, the measured value of $|B/A|$ is $0.89 \pm 0.08 \pm 0.09 \text{ GeV}^{-1/2}$; the systematic error is due to the background description 3 %. Figure 4 shows that $|B/A|$ does not vary significantly as a function of rapidity. Since rapidity is related to photon energy (Eq. 1) this also shows that there is no significant variation with photon energy. This $|B/A|$ ratio also appears to be independent of the polar and azimuthal angle, as expected.

Our measured value for $|B/A|$ is in agreement with the previous STAR result, $|B/A| = 0.81 \pm 0.08 \pm 0.20 \text{ GeV}^{-1/2}$ [4]. The ZEUS studies of $\gamma p \rightarrow \rho p$ find $|B/A| = 0.67 \pm 0.03 \text{ GeV}^{-1/2}$ [23] for $t < 0.5 \text{ GeV}^2$. After the extrapolation of the ZEUS measured t dependence of $|B/A|$ to our average value of t , we get $|B/A| \approx 0.8$, consistent with our results. This decrease of $|B/A|$ with increasing $|t|$ and independence of the polar and azimuthal angle is expected [18].

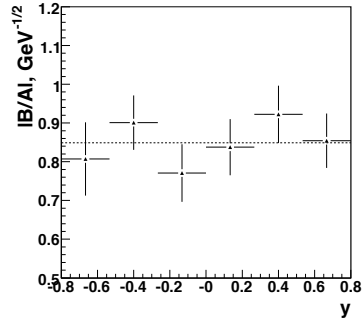


FIG. 4: The ratio $|B/A|$ as the function of y_ρ obtained by fitting the Eq.3 to the invariant mass distributions in bins of y_ρ .

E. Cross Section - $d\sigma/dy_\rho$ and $d\sigma/dt$ for Minimum Bias events

The differential cross section was studied as a function of rapidity and p_T^2 . The minimum bias efficiency-corrected $d\sigma/dy$ is shown in Fig 5. This was obtained by fitting the invariant mass distribution of the ρ^0 candidates separated in bins of rapidity. The distribution for each rapidity bin was fitted by Eq. 3 and the ρ^0 yield extracted; direct $\pi\pi$ are not included in the yield. Also shown is a prediction of the Klein-Nystrand model; unfortunately, the other two models do not include nuclear excitation.

Fig. 6 shows the $p_T^2 = t_\perp$ spectrum for the minimum bias data after efficiency correction and luminosity normalization. Since the longitudinal momentum transfer from the target nucleus $t_{||} = m_V^2/2k$ is small ($\approx 2 \text{ MeV}^2$ at mid-rapidity), $t \approx t_\perp$. As with $d\sigma/dy$, each t_\perp bin was fitted to Eq. 3 to extract the ρ^0 yield.

We do not observe the dip for $0.01 < t < 0.015 \text{ GeV}^2$ predicted by FSZ [7]. However, that model does not include the photon p_T in the calculation; this will diminish the size of the diffractive dips [24].

The $d\sigma/dt_\perp$ distribution (summed over $|y_{\rho^0}| < 1$) is fit to a sum of two exponentials, for coherent and incoherent scattering:

$$\frac{d\sigma}{dt} = A_{coh} \exp(-B_{coh} t_\perp) + A_{inc} \exp(-B_{inc} t_\perp). \quad (4)$$

Although this simple fit function is appealing, it has several drawbacks. First, interference between ρ photoproduction on the two nuclei reduces $d\sigma/dt$ at small t [10, 24], and, in fact, alters the minimum-bias t -spectrum at the 20 % level for $t < 0.01 \text{ GeV}^2$. Also, incoherent production is reduced at small t [25]. Despite these drawbacks, we use this fit to describe our data.

We perform two fits to the data. The first, a fit over all t values yields exponentials that should be integrable to give the total coherent cross-section, shown in the left column of the Table I. Because of the interference, it has a poor χ^2/DOF , 79.12/10. The second fit is performed over the p_T^2 range (0.002,0.3) GeV^2 , avoiding the region where the interference is large. While interference is still non-negligible, this fit has a marginally acceptable χ^2/DOF , 8.1/7. This fit should yield a usable nuclear slope, with accuracy comparable to other experiments. Both fits give similar results for the incoherent production.

With the 2nd fit, we find the coherent production slope obtained with double exponential fit function is $B_{coh} = 388 \pm 24 \text{ GeV}^{-2}$. For direct comparison with previous STAR results, we also tried a single exponential fit function which gives $B_{coh} = 363 \pm 21 \text{ GeV}^{-2}$, in agreement with that observed at 130 GeV , $358 \pm 31 \text{ GeV}^{-2}$ [4]. These numbers are not directly comparable with fixed-target photoproduction data because, in UPC photoproduction, the photon flux is higher on the side of the target nearest the photon emitter, and lower on the far side of

TABLE I: Parameters for the fit to to the $d\sigma/dt$, Eq. (4).

Parameter	t range (0.,0.3)	t range (0.002,0.3)
A_{coh} , mb/ GeV^2	1050 ± 57	2307 ± 258
B_{coh} , GeV^{-2}	-256 ± 12	-388 ± 24
A_{inc} , mb/ GeV^2	21.6 ± 2.4	24.8 ± 2.5
B_{inc} , GeV^{-2}	-7.9 ± 0.9	-8.8 ± 1.0

the target. The photon flux falls as $1/r^2$, so this leads to a slightly smaller apparent source size.

The incoherent slope, $B_{inc} = 8.8 \pm 1.0 \text{ GeV}^{-2}$ has not previously been studied in heavy-ion collisions. However, it is comparable to the slope observed by STAR in dAu collisions [26], and comparable to the ZEUS $b = 10.9 \pm 0.3 \text{ (stat.)}^{+1.0}_{-0.5} \text{ (syst.)} \text{ GeV}^{-2}$ [23] and H1 results $b = 10.9 \pm 2.4 \text{ (stat.)} \pm 1.1 \text{ (syst.)} \text{ GeV}^{-2}$ [27] for ρ^0 photoproduction on proton targets at comparable t values. The HERA data is at higher $W_{\gamma N}$, but the energy difference is not expected to introduce a large shift.

The two exponentials in Eq. 4 may be analytically integrated to find the total coherent and incoherent cross sections. This approach neglects corrections due to the loss of incoherent cross-section when the coherent cross-section is large [25], but is useful for phenomenological comparisons. For $|y_{\rho^0}| < 1$, we find the ratio $\sigma_{incoherent}/\sigma_{coherent} = 0.29 \pm 0.03 \pm 0.03$ for events with mutual excitation (Xn,Xn).

We have also studied the cross-sections for ρ^0 production accompanied by single neutron emission (1n,1n); this is largely due to mutual excitation to Giant Dipole Resonances. This is done by fitting the ZDC spectra in Fig. 2 and extracting the single neutron component. For $|y_{\rho^0}| < 1$, we find $\sigma_{incoherent}^{1n1n}/\sigma_{coherent}^{1n1n} = 0.18 \pm 0.08 \pm 0.02$. The higher $\sigma_{incoherent}/\sigma_{coherent}$ for the $XnXn$ sample may signal a breakdown of the factorization implicit in Eq. 2, possibly because the incoherent ρ production transfers enough energy to dissociate the target nucleus; this largely leads to multiple neutron emission [28].

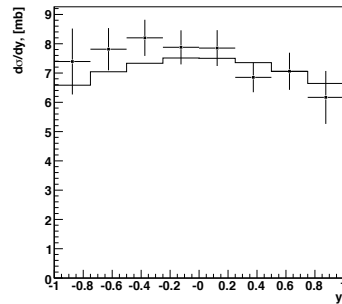


FIG. 5: Coherent ρ^0 production cross section as the function of y_ρ (black triangles) overlapped by the normalized dN/dy distribution obtained with KN model (solid line).

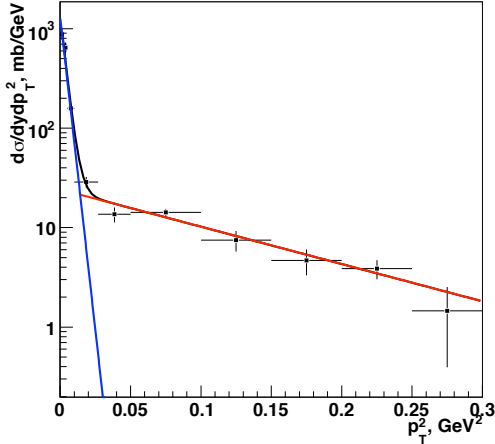


FIG. 6: ρ^0 production cross section as a function of p_T^2 , together with the fit to Eq. 4. The fit parameters are shown in Table I.

F. Cross Sections

Three theoretical models [6, 7, 9] which provide predictions for the ρ^0 production cross section have been compared with the available ρ^0 production cross section measurements as a function of rapidity. This comparison is shown in Fig. 7. The measured distribution is obtained by scaling cross section distribution for $XnXn$ with scaling factors $\sigma(\rho_{0n0n})/\sigma(\rho_{XnXn})$ and $\sigma(\rho_{0nXn})/\sigma(\rho_{XnXn})$ as a function of rapidity. The scaling is needed because the efficiency of the topology trigger is poorly known. Therefore the ρ^0 production cross section for the events with mutual excitation measured with minimum bias sample has been extrapolated based on the ratios $\sigma(0n0n)/\sigma(XnXn) = 7.1 \pm 0.3$ and $\sigma(0nXn)/\sigma(XnXn) = 3.5 \pm 0.2$ which are measured within the topology sample. Due to the limited acceptance in rapidity, we cannot distinguish between the different theoretical models based on the shape. However the total production cross section can be used to eliminate models which significantly overestimate the total production cross section in the measured rapidity range.

The cross-sections for coherent and incoherent production for $|y_\rho| < 1$ accompanied by nuclear excitation are $\sigma_{coh}(XnXn, |y_\rho| < 1) = 14.5 \pm 0.7 \pm 2.2$ mb and $\sigma_{inc}(XnXn, |y_\rho| < 1) = 4.3 \pm 0.5 \pm 0.7$ mb.

Finding the total cross sections requires an extrapolation to the region $|y_\rho| > 1$, which is necessarily model dependent. The KN [29] and FSZ [7] calculations have a similar $d\sigma/dy$ distributions, so a single extrapolation should work well for them. For the KN calculation, the extrapolation factor from $\sigma(|y_\rho| < 1)$ to σ_{tot} is 2.2 for the events with nuclear break-up. We assume that this factor is the same for coherent and incoherent production. It should be noted that, at large p_T (large compared to

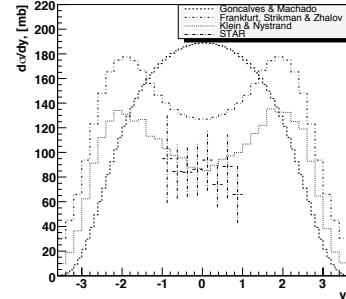


FIG. 7: Comparison of theoretical predictions to the measured spectra for the coherent ρ^0 production cross section (statistical and systematical errors are indicated).

$mv/2$), the p_T can affect the relationship between photon energy and ρ^0 rapidity, possibly changing the extrapolation factor. The coherent production cross section extrapolated to the full rapidity range is $\sigma_{coh}(XnXn, total) = 31.9 \pm 1.5 \pm 4.8$ mb. The total cross section is

$$\sigma_{coh+inc}(XnXn, total) = 41.4 \pm 2.9 \pm 5.1 \text{ mb}; \quad (5)$$

the $XnXn$ denotes the requirement of neutron emission due to nuclear dissociation.

For ρ^0 production accompanied by single neutron emission, we find, $\sigma_{coh}(1n1n, |y_\rho| < 1) = 1.07 \pm 0.08 \pm 0.09$ mb and $\sigma_{inc}(1n1n, |y_\rho| < 1) = 0.21 \pm 0.09 \pm 0.03$ mb.

The extrapolation factor from $|y_\rho| < 1$ to 4π is similar to that for the $XnXn$ dataset, 2.2. The total cross section for single neutron emission is

$$\sigma_{coh+inc}(1n1n, total) = 2.8 \pm 0.3 \pm 0.2 \text{ mb} \quad (6)$$

Based on the ratio $\sigma(\rho_{0n0n})/\sigma(\rho_{XnXn})$, we find $\sigma_{coh}(0n0n, |y_\rho| < 1) = 102.9 \pm 4.9 \pm 15.6$ mb.

As with the $XnXn$ data, the extrapolation to 4π is model dependent. For the KN model, the extrapolation factor is 3.7. For the FSZ model, the factor would be 3.5, and for the saturation model GM [9], 2.13. The KN and FSZ model factors are similar, and since the KN $d\sigma/dy$ matches the $XnXn$ data well, we adopt an overall extrapolation factor of 3.6 ± 0.1 . With that, we find $\sigma_{coh}(0n0n, total) = 380 \pm 18 \pm 58$ mb and total cross section for events with $0n0n$ (coherent, incoherent) is

$$\sigma_{coh+inc}(0n0n, total) = 494 \pm 23 \pm 59 \text{ mb} \quad (7)$$

It is also possible for a single nucleus to be excited, $0nXn$ in this language. We have checked that we get symmetric results for this channel when the signals are in the east or west ZDC. The possibilities are added linearly.

This yields the total coherent cross section $\sigma_{coh}(AuAu \rightarrow Au^*Au^*\rho^0) = 517 \pm 19 \pm 108$ mb, and total cross section (coherent, incoherent)

$$\sigma_{coh+inc}(AuAu \rightarrow Au^*Au^*\rho^0) = 680 \pm 26 \pm 144 \text{ mb}. \quad (8)$$

The measured coherent and incoherent production cross sections compared with results obtained at $\sqrt{s_{NN}}$

TABLE II: Coherent ρ^0 production cross section at $\sqrt{s_{NN}} = 200$ GeV accompanied by nuclear breakup and without breakup compared with previous measurements at $\sqrt{s_{NN}} = 130$ GeV [4]

Parameter	STAR at $\sqrt{s_{NN}} = 200$ GeV	STAR at $\sqrt{s_{NN}} = 200$ GeV	STAR at $\sqrt{s_{NN}} = 130$ GeV
	coherent	coherent + incoherent	coherent
σ_{XnXn}^{ρ} (mb)	$31.9 \pm 1.5 \pm 4.8$	$41.4 \pm 2.9 \pm 5.1$	$28.3 \pm 2.0 \pm 6.3$
σ_{0nXn}^{ρ} (mb)	$105 \pm 5 \pm 16$	$145 \pm 7 \pm 28$	$95 \pm 60 \pm 25$
σ_{1n1n}^{ρ} (mb)	$2.4 \pm 0.2 \pm 0.2$	$2.8 \pm 0.3 \pm 0.2$	$2.8 \pm 0.5 \pm 0.7$
σ_{0nnn}^{ρ} (mb)	$380 \pm 18 \pm 58$	$494 \pm 23 \pm 59$	$370 \pm 170 \pm 80$
σ_{total}^{ρ} (mb)	$517 \pm 19 \pm 108$	$680 \pm 24 \pm 144$	$460 \pm 220 \pm 110$

$= 130$ GeV [4] is summarized in Table II. The measured increase in photoproduction cross section with energy is much slower than proposed in [8] and [9].

Several sources of systematic error have been considered in the analysis. The main source of the systematic errors for the cross section in the rapidity range $|y_{\rho^0}| < 1$ are luminosity 10 %, applied cuts and fit function 7 %. The major systematic errors for the total coherent and incoherent production cross section are luminosity 10 % and extrapolation to the full rapidity 15 %. Those uncertainties were added in quadrature to give the systematical errors for the production cross section.

G. ρ^0 Spin Density Matrix

The angular distribution allows a determination of the ρ^0 spin density matrix elements. In order to measure those elements a two dimensional correlation of angle Φ_h vs $\cos(\Theta_h)$, of the produced π^+ in the ρ^0 helicity frame, has been produced. Θ_h is defined as the polar angle between beam direction and direction of π^+ in the ρ^0 rest frame. The azimuthal angle Φ_h is the angle between the decay plane and the ρ^0 production plane. Production plane of ρ^0 contains ρ^0 and virtual photon. The dependence of the cross section on Φ_h and $\cos(\Theta_h)$ can be written as follows:

$$\frac{1}{\sigma} \frac{d\sigma}{dcos(\Theta_h)d\Phi_h} = \frac{3}{4\pi} \left[\frac{1}{2}(1 - r_{00}^{04}) + \frac{1}{2}(3r_{00}^{04} - 1) \cos^2(\Theta_h) - \sqrt{2}\Re[r_{10}^{04}] \sin(2\Theta_h) \cos(\Phi_h) - r_{1-1}^{04} \sin^2(\Theta_h) \cos(2\Phi_h) \right] \quad (9)$$

The three spin density matrix elements $r_{00}^{04}, r_{10}^{04}, r_{1-1}^{04}$ can be extracted by fitting the two dimensional correlation. The element r_{00}^{04} represents the probability that the ρ^0 is produced with helicity 0 from a photon with helicity ± 1 . The element r_{1-1}^{04} is related to the size of the interference between the helicity non flip and double flip and $\Re[r_{10}^{04}]$ is related to the interference of non-flip to single flip. If helicity conservation holds, then all three matrix elements have to be close to zero.

Figure 8 shows the fitted Φ_h vs $\cos(\Theta_h)$ correlation. The measured spin density matrix elements are shown in the Table III. The method used is to fit the invariant

TABLE III: Measured spin density matrix elements compared with γp experiment results

Parameter	Fit result	γp experiment [23]
χ^2/ndf	26/21	
r_{00}^{04}	$-0.03 \pm 0.03 \pm 0.06$	0.01 ± 0.03
$\Re[r_{10}^{04}]$	$0.04 \pm 0.02 \pm 0.03$	0.01 ± 0.02
r_{1-1}^{04}	$-0.01 \pm 0.03 \pm 0.05$	-0.01 ± 0.02

mass distributions in bins of Φ_h and $\cos(\Theta_h)$ to determine the yield in each bin. The background is accounted in the fitting function as described in section III A. The main source of the systematic uncertainty is how the background is being estimated, to do this we use alternative approach of estimating the background using scaled like-sign pairs. This distribution is then subtracted from that for opposite-sign pairs. Additional source of systematic error is the uncertainty due to the acceptance correction and therefore the ρ^0 simulation. Also, we estimate the systematic error obtained from varying the bin size of the angular correlation. The systematic error for the spin density matrix elements is obtained by adding the individual uncorrelated contributions in quadrature. The measured ρ^0 helicity matrix elements indicates that helicity is conserved within errors as expected based on s-channel helicity conservation.

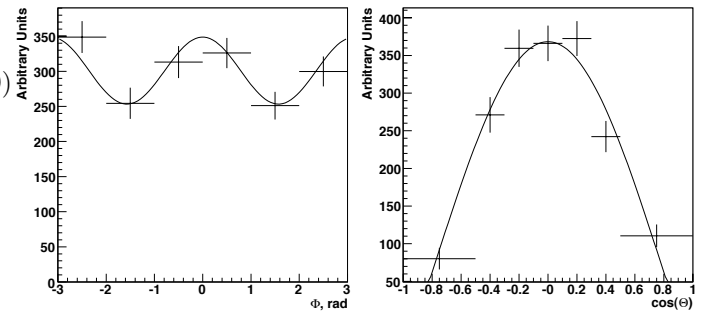


FIG. 8: Projection of the two dimensional efficiency corrected Φ_h vs $\cos(\Theta_h)$ distributions. The solid line shows the result of the two-dimensional fit to the data with Eq. 9 and the coefficients given in Tab. III

IV. CONCLUSION

Photoproduction of ρ^0 mesons has been measured in the STAR detector at RHIC in relativistic heavy ion collisions at $\sqrt{s_{NN}} = 200$ GeV. Coherent and incoherent ρ^0 production have been observed. Also production of the ρ^0 mesons is observed with and without accompanying Coulomb nuclear excitations. The measured increase in photoproduction cross section with energy is much slower than proposed in [8] and [9]. The model [6] is able to describe the data for two energy points $\sqrt{s_{NN}} = 130$ and 200 GeV.

The differential cross section has been studied as a function of p_T^2 , y_ρ and $M_{\pi\pi}$. The $d\sigma/dp_T^2$ distribution was fitted with a double exponential function to isolate the incoherent production and allow the measurement of the nuclear radius.

The ratio $|B/A|$ has been studied with respect to polar, azimuthal angle and y_ρ ; no dependence has been observed as predicted [18].

The r_{00}^{04} , $\Re r_{10}^{04}$ and r_{1-1}^{04} spin density matrix elements for the ρ^0 meson were obtained. The small values of

r_{00}^{04} , $\Re r_{10}^{04}$ and r_{1-1}^{04} indicate that helicity is conserved within errors as expected based on spin channel helicity conservation (SCHC). We see no evidence for ρ photo-production involving spin flip.

Acknowledgments

We thank the RHIC Operations Group and RCF at BNL, and the NERSC Center at LBNL for their support. This work was supported in part by the Offices of NP, HEP and EPSCOR within the U.S. DOE Office of Science; the U.S. NSF; the BMBF of Germany; CNRS/IN2P3, RA, RPL, and EMN of France; EPSRC of the United Kingdom; FAPESP of Brazil; the Russian Ministry of Science and Technology; the Ministry of Education and the NNSFC of China; IRP and GA of the Czech Republic, FOM of the Netherlands, DAE, DST, and CSIR of the Government of India; Swiss NSF; the Polish State Committee for Scientific Research; SRDA of Slovakia, and the Korea Sci. & Eng. Foundation.

-
- [1] G. Baur *et al.*, Phys. Rep. **364**, 359 (2002); F. Krauss, M. Greiner and G. Soft, Prog. Part. Nucl. Phys. **39**, 503 (1997) C. Bertulani, S. Klein, J. Nystrand; Ann. Rev. Nucl. Part. Sci. **55**, 271 (2005).
 - [2] C.F. v. Weizsaecker, Z. Phys. **88**, 612 (1934); E.J. Williams, Phys. Rev. **45**, 729 (1934).
 - [3] F. Bulos *et al.*, Phys. Rev. Lett. **10**, 490 (1969); H. Alvensleben *et al.*, Phys. Rev. Lett. **24**, 786 and 792 (1970), and Nucl. Phys. **B18**, 333 (1970); G. McClellan *et al.*, Phys. Rev. **D4**, 2683 (1971).
 - [4] C. Adler *et al.*, Phys. Rev. Lett. **89**, 272302 (2002).
 - [5] David d'Enterria (for the PHENIX Collaboration); nucl-ex/0601001.
 - [6] S. Klein, J. Nystrand Physical Review **C60** 014903 (1999).
 - [7] M. Frankfurt; M. Strikman, M. Zhalov, Phys. Rev. **C67**, 034901 (2003); M. Frankfurt; M. Strikman, M. Zhalov, Phys. Lett. **537**, 51 (2002).
 - [8] M. Frankfurt; M. Strikman, M. Zhalov, hep-ph 0204175.
 - [9] V.P. Goncalves, M.V.T. Machado, Eur.Phys.J. **C40** 519, (2005).
 - [10] J. Nystrand, A. Baltz and S. Klein Phys. Rev. Lett. **89**, 012301 (2002).
 - [11] G. Baur *et al.*, Nucl. Phys. **A729**, 787 (2003).
 - [12] C. Bertulani, S. Klein, J. Nystrand, Ann. Rev. Nucl. Part. Sci. **55** 271-310, (2005).
 - [13] K. Schilling *et al.*, Nucl. Phys. **B15**, 397 (1970); K. Schilling and G. Wolf, Nucl. Phys. **B61**, 381 (1973).
 - [14] A. Airapetian *et al.*, Phys. Lett. **B513**, 301 (2001), E665 Collaboration, M.R. Adams *et al.*, Z. Phys. **C74**, 237 (1997), W.D. Shambroom *et al.*, CHIO Coll., Phys. Rev. **D26** 1 (1982).
 - [15] M. Anderson *et al.*, Nucl. Instrum. and Methods **A499**, 659 (2003);
M. Anderson *et al.*, Nucl. Instrum. and Methods **A499**, 679 (2003).
 - [16] C. Adler, *et al.*, Phys. Rev. **C70**, 031902(R) (2004).
 - [17] A.J.Baltz, C.Chasman, S.N.White, Nucl. Instrum. Meth. **A417**, 1 (1998).
 - [18] M.G.Ryskin, Yu.M.Shabelski; Yad. Fiz. **61**, 89 (1998).
 - [19] J. Breitweg *et al.*, Eur Phys J **C2**, 247 (1998).
 - [20] P. Söding Phys. Rev Lett. **19**, 702 (1966).
 - [21] J.J. Sakurai, Ann. Phys. **11**, 1 (1960); T.H. Bauer *et al.*, Rev. Mod. Phys. **50**, 261 (1978).
 - [22] Particle Data Group, C. Caso *et al.*, Europ. Phys. Jour. **C3**, (1998).
 - [23] ZEUS Collaboration; The European Physical Journal **C2**, 247 (1998).
 - [24] S. Klein and J. Nystrand, Phys. Rev. Lett. **84**, 2330 (2000).
 - [25] G. V. Bochmann, B. Margolis and C. L. Tang, Phys. Lett. **B30**, 254 (1969).
 - [26] S. Timoshenko (for the STAR Collaboration), nucl-ex/0701077.
 - [27] S. Aid *et. al.*, Nucl. Phys. **B463**, 3 (1996).
 - [28] M. Strikman, M. Tverskoy and M. Zhalov, Phys. Lett. **B626**, 72 (2005).
 - [29] J. Nystrand, S. Klein; nucl-ex/9811007.